# Statistical characteristics of flow as indicators of channeling in heterogeneous porous and fractured media

R. Le Goc [a,b], J.-R. de Dreuzy [a] and P. Davy [a]

[a] Géosciences Rennes, UMR 6118 CNRS, Université de Rennes 1, CS 74205, F-35042 Rennes Cedex, FRANCE

[b] Itasca Consultants SAS, 64 chemin des mouilles, F-69134, Écully Cedex, FRANCE

**Abstract**

We introduce two new channeling indicators $D_{ic}$ and $D_{cc}$ based on the Lagrangian distribution of flow rates. On the basis of the participation ratio, these indicators characterize the extremes of both the flow-tube width distribution and the flow rate variation along flow lines. The participation ratio is an indicator biased toward the larger values of a distribution and is equal to the normalized ratio of the square of the first-order moment to the second-order moment. Compared with other existing indicators, they advantageously provide additional information on the flow channel geometry, are consistently applicable to both porous and fractured media, and are generally less variable for media generated using the same parameters than other indicators. Based on their computation for a broad range of porous and fracture permeability fields, we show that they consistently characterize two different geometric properties of channels. $D_{ic}$ gives a characteristic scale of low-flow zones in porous media and a characteristic distance between effectively flowing structures in fractured cases. $D_{cc}$ gives a characteristic scale of the extension of high-flow zones in porous media and a characteristic channel length in fractured media. $D_{ic}$ is mostly determined by channel density and permeability variability. $D_{cc}$ is, however, more affected by the nature of the correlation

structure like the presence of permeability channels or fractures in porous media and the length distribution in fracture networks.

*Keywords:* flow channels; heterogeneous media; connectivity; fracture network; channeling indicators

## 1. Introduction

Spatial heterogeneity in hydraulic conductivity affects fluid flow and solute transport in complex natural media like fractured media [38], alluvial systems [11] and strongly heterogeneous porous media [28] and has been a subject of research for decades ([8] and references therein). It is a function of contrasts between high permeability and low permeability values. As flow tends to avoid low-*k* zones for high-*k* zones, heterogeneity induces the development of preferential flow paths [20,23] also called "paths of least resistance" [39], along which flow is focused. Their effects on upscaled/effective hydrologic properties have been observed in laboratory and numerical studies. *Fogg* [10] performed a numerical study on the hydraulic conductivity distribution in the Wilcox aquifer and suggests that flow is mainly controlled by the continuity and connectivity of sand deposits rather than by local hydraulic conductivity values. *Hanor* [16] drew similar conclusions for the Livingston site. *Silliman* [34] illustrated the formation of preferential flow paths with laboratory experiments. [22,30] showed how the estimate of aquifer properties, like the effective permeability of a system, should take channeling into account. *Ronayne et al.* [31] used statistical channeling properties to estimate aquifer parameters in a system affected by channeling. Similarly, *Kerrou et al.* [19] showed that not accounting explicitly for channeling in a sequential self-calibration approach resulted in flow underestimation and strong deviations in capture zone estimates. *Trinchero et al.* [37] showed that for moderate heterogeneities, both the connectivity of high-*k* values and apparent porosity are key in predicting transport times efficiently. Although channeling is important for flow and transport properties, its quantification remains a matter of debate. Two types of indicators have been proposed: indicators derived from the comparison of upscaled hydraulic properties with their small-scale counterparts, and statistical indicators calculated from the permeability and flow

53 fields. The first category of estimators is based on hydraulic properties that are sensitive to
54 channeling. The simplest estimator is the effective permeability, $K_{eff}$, known to be sensitive to
55 flow organization [14]. In 2D multi-log-Gaussian isotropic weakly-correlated fields, the
56 equivalent permeability is equal to the geometric mean $K_{eff}$=$K_g$ [27]. If the connectivity of the
57 higher-$K$ zones is greater than that of the lower-$K$ zones, $K_{eff}$ is larger than $K_g$ [32] within the
58 limit that $K_{eff} \leq K_a$ (where $K_a$ is the arithmetic mean) [40]. The type of average measured by
59 the power averaging exponent $CF_1$ [9,18] has thus been considered as a measure of
60 channeling [20]:

$$CF_1 : K_{\text{eff}} = \left(\frac{1}{V}\int_V K(x)^{CF_1} dV\right)^{\frac{1}{CF_1}} \quad (1)$$

61 $CF_1$ varies between -1 and 1 for the harmonic and arithmetic means, respectively, and is equal
62 to zero for the geometric mean corresponding to isotropic weakly-correlated multi-Gaussian
63 fields. As transport is also strongly affected by channeling, breakthrough curve properties
64 have been proposed as estimators of the channeling degree [41]. *Knudby and Carrera* [20]
65 used the ratio $CT_1$ of the average arrival time $\bar{t}$ to the time at which 5% of the solute have
66 broken through the domain boundary $t_5$:

$$CT_1 = \bar{t}/t_5. \quad (2)$$

67 When preferential flow paths exist, $t_5$ becomes much smaller than $\bar{t}$, $CT_1$ increases and the
68 field should be considered as increasingly connected. The apparent hydraulic diffusivity has
69 been proposed as an intermediary characteristics between flow and transport connectivities
70 [21]. *Park et al.* [29] suggested that the normalized travel time and distance be used to
71 investigate preferential flow.

72 The second category of estimators uses statistical characteristics of the permeability field or of
73 the flow field. *N*-point spatial connectivity statistics are dedicated to the measurement of
74 connectivity and were applied to permeability fields to estimate the presence of high-*k*
75 connected patterns [17,24]. *Western et al.* [42] used a directional multi-point geostatistical
76 indicator and showed that it could capture the difference between random and channeled
77 fields with similar *k*-distributions, unlike non-directional indicators. *Frippiat et al.* [13]
78 suggested that the presence of preferential flow paths or flow barriers could be identified
79 using head and flow variances, since head variance is negatively correlated to connectivity
80 while flow variance is positively correlated to the effective permeability increase. *Bruderer-*
81 *Weng et al.* [3] used the multifractal spectrum of the flow field to quantify channeling in
82 heterogeneous pipe networks. The distribution of flow has also been used for quantifying
83 channeling in fractured networks [6].

84 The multiplicity of the proposed indicators shows that channeling cannot be restricted to a
85 single simple characteristic. The concept of channeling also strongly depends on the
86 application targeted. The relevant use of channeling indicators probably differ between flow
87 and transport applications [33]. In this study, we focused first on the geometrical
88 characterization of channels, i.e. on the channels themselves rather than on their consequences
89 in terms of flow or transport. In this respect, the first category of indicators based on
90 equivalent medium properties are limited by the fact that they measure the consequences of
91 channeling rather than channeling itself. The limitation of the indicators based on
92 permeability statistics arises from the measurement of a single cause of channeling cause (the
93 connectivity of high-*K* zones) where channeling is also induced by the variability of
94 permeability [26]. The advantage of those indicators based on the statistical properties of the
95 flow field is the measurement of channeling itself. As opposed to the multifractal dimensions
96 and the variance of head or flow, we look for indicators based on the geometrical properties of

97 the channels that additionally identify channeling consistently in both porous and fractured
98 media.

99 Even though channeling occurs under many different circumstances, it has two recurrent
100 characteristics. First, flow is localized within a few structures. Second, channeling locally
101 maintains high flow rates over long distances. On the basis of these two characteristics, we
102 aimed at defining quantitative channeling indicators that met the three following constraints.
103 First, they must be globally consistent with the visually intuitive classification of channeling.
104 Second, they must provide a quantification of channeling. Third, they must be applicable
105 simultaneously to porous and fractured media.

106 We define two new indicators in section 2. We compute their value for the broad range of
107 synthetic fields introduced in section 3. In section 4, we analyze first their consistency with
108 the expected ranking of channeling and then their dependency on the permeability correlation
109 structures. Finally, we compare them to other existing indicators in section 5.

110 ## 2. Flow-based indicators

111 A channeled medium is defined as a medium where flow is localized within a few structures
112 and where preferential flow locally maintains high flow rates over long distances. To this end,
113 we defined two channeling indicators, one quantifying the localization of flow within the
114 system and the other quantifying the continuity of flow paths. Since the proposed indicators
115 were not straightforward, we introduce them using preliminary attempts based on simpler
116 quantities. The objective was to show the relevance of the more complex indicators finally
117 adopted. The first indicator should characterize the relative volume occupied by the high-flow
118 zones. The simplest indicator could be the relative volume occupied by flows larger than a
119 given threshold value. Although simple, this indicator depends on the arbitrary choice of the
120 threshold value. Rather than a deterministic indicator, we looked for a statistical characteristic

biased toward the higher values of the flow distribution. Since the moments of the flow distribution $M_k(\Phi)$ are increasingly sensitive to the highest values with increasing orders $k$, the idea was to compare moments of increasing orders like in the participation ratio $S_2$ [5,35] equal to :

$$S_2(\Phi) = M_1(\Phi)^2/(M_0(\Phi)\cdot M_2(\Phi)) \quad (3)$$

where $\Phi$ stands for the spatial distribution of flow rates. For $\Phi$ discretized on a domain of $n$ cells of volumes $V_i$, $M_k(\Phi)$ writes:

$$M_k(\phi) = \sum_{i=1}^{n} {\varphi_i}^k \times V_i \quad (4)$$

where $\varphi_i$ is the mean value of $\Phi$ over the grid cell $i$. Table 1 shows $S_2$ values for usual distributions. When the distribution variability vanishes, $S_2$ tends to 1. By contrast, $S_2$ systematically decreases with higher variability whatever the distribution type. For the lognormal distribution, $S_2$ is solely function of the lognormal variance.

Whereas $S_2(\Phi)$ gives indications about the surface occupied by the largest flow rates, it does not account for the distribution of this surface within the domain. Consequently, we did not use $S_2(\Phi)$ but $S_2(W_n)$, where $W_n$ is the distribution of flow-tube widths carrying all the same fraction $1/n$ of the total flow. Since $S_2(W_n)$ is biased toward the larger $W_n$ values , it characterizes the extension of the low-flow zones and hence the distance between main flow channels. We defined and computed $W_n$ in the specific context of permeameter-like boundary conditions defined for a square domain by fixed heads on two opposite sides and no flow on the other sides. The definition of $W_n$ may also be adapted for different boundary conditions. In convergent flow conditions, $W_n$ would be defined by the distance between flow lines normalized by the distance to the well. With permeameter-like boundary conditions, we first

141 determined $n$ equivalent flow tubes defined as the tubes carrying all the same fraction $1/n$ of
142 the total flow (Figure 1, middle column). Then, we computed the participation ratio $S_2(W_n)$ on
143 the flow-tube width distribution.

144 We introduce the meaning of $S_2(W_n)$ with the case of $p$ regularly spaced flow tubes of width
145 $L/p$, where $L$ is the system size, and $n$-$p$ flow tubes of negligible width within the channels.
146 The distribution of flow-tube widths is thus a binary distribution of values $L/p$ with a
147 probability $p/n$, and 0 with a probability $(1-p/n)$. From Table 1, it leads to $S_2(W_n)=p/n$. In this
148 case, $S_2(W_n)$ is directly proportional to the number of channels $p$. When the number of
149 channels $p$ is equal to $n$, $S_2(W_n)$ reaches a value of 1, like in homogeneous flow fields. In fact,
150 for a homogeneous case, all flow tubes have the same width and $S_2(W_n)=1$. Using this same
151 example, we derived the characteristic distance between channels $D_{ic}$ from $S_2(W_n)$. Since the
152 distance between two channels is equal to $D_{ic}=L/p$ and $S_2(W_n)=p/n$, then:

$$\frac{D_{ic}}{L} = \frac{1}{n \cdot S_2(W_n)} \tag{5}$$

153 $D_{ic}$ ranges from $L/n$ in homogeneous fields to $L$ in a unique channel conveying all the flow,
154 for which $S_2(W_n)=1/n$. $L/n$ can be a priori interpreted as a channel resolution. The selection of
155 an appropriate value for $n$ will be investigated at the beginning of section 4. $D_{ic}$ is a
156 characteristic distance between channels. However, it does not provide any information on
157 the channel persistence throughout the system. For example, in Figure 1 the field at the top
158 and the field in the middle have two different flow fields with about the same $D_{ic}/L$ ratio equal
159 to 0.09, but high flow rates are visually maintained over a longer distance in the middle field
160 than in the top field.

161 We looked for a second indicator designed to differentiate these two fields by characterizing
162 the distance over which flow rates are continuously high. We first tried the Lagrangian

correlation length of flow rates. It was however not consistent with our intuition of channel persistency. For example, the correlation length of the rearranged field in Figure 1 (middle) is smaller than the correlation length of the non-rearranged field (Figure 1, top). The correlation length is not only sensitive to the large flow rates but also to all other values. It thus fails to characterize high-flow zone connectivity. Like for the previous indicator, computing the Lagrangian correlation length from the sole velocities larger than a given threshold faces the same problem of the arbitrary choice of the threshold. Moreover, the channels may display some discontinuities that hinder the relevance of a threshold (Figure 1, right bottom). We found that characterizing flow channel discontinuities is easier than flow channel persistence since discontinuities are more localized. Large values of the spatial derivatives of flow rates are more localized at the entrance and exit of channels than in the remaining of the field. On the contrary, the variations of flow rates are smaller and distributed evenly in non-channeled media. To characterize the distribution of the flow transitions taken as the Lagrangian derivatives of flow rates $\Phi'$, we used again the participation ratio $S_2$ on $\Phi'$ (right column in Figure 1). Numerically, $S_2(\Phi')$ was calculated according to (3) from the moments of the distribution of $\Phi'$ discretized along the flow lines:

$$M_k(\Phi') = \sum_{j=1}^{p} \sum_{i=1}^{m} \Delta s_i^j \left| \frac{\Delta \varphi_i^j}{\Delta s_i^j} \right|^k \tag{6}$$

with $j$ the flow line index, $p$ the number of flow lines, $s_i^j$ the $i^{\text{th}}$ position along the flow line $j$, $m$ the number of positions along the flow line, $\Delta\varphi_i^j$ and $\Delta s_i^j$ the flow rate variation and distance between two consecutive points. Flow lines were computed by using a particle-tracking algorithm. We chose $p$ equal to $10^4$ and $m$ so that $\Delta s_i^j$ was of the order of the grid cell size after ensuring that larger $p$ and $m$ values did not modify the results. $S_2(\Phi')$ defines a characteristic distance $l_{\text{eff}}$ over which flow rates are actually variable divided by the average

flow line length ($L'$) [35]. By contrast, a characteristic scale $D_{cc}$ over which flow rates are only slowly varying is function of $L'$-$l_{eff}$:

$$D_{cc}/L' = (L'-l_{eff})/L' = (1-S_2(\Phi')) \quad (7)$$

$D_{cc}$ will be taken as a characteristic channel length. In media with discontinuous flow paths, $\Phi'$ has a narrow and spatially uniform distribution, leading to $S_2(\Phi')=1$ and $D_{cc}/L' = 0$. In highly-channeled media, the distribution $\Phi'$ contains values close to zero except at the channel extremities, leading to small $S_2(\Phi')$ values and $D_{cc}/L'$ close to 1. For example, the $D_{cc}/L'$ value for the middle field in Figure 1 is equal to 0.72. It is larger than the value of 0.43 for the field at the top of Figure 1 following the intuition that persistence is larger in the middle field.

$D_{ic}/L$ and $D_{cc}/L'$ are statistically-derived indicators designed to characterize flow localization and flow continuity. They are dimensionless quantities ranging between 0 and 1 that can be used to compare channeling in different systems. In section 3, we define a broad range of synthetic porous fields and fracture networks in which $D_{ic}$ and $D_{cc}$ will be computed in section 4.

## 3. Tested media and computational methods

Indicators $D_{ic}$ and $D_{cc}$ will be compared in the different synthetic fields displaying various connectivity degrees presented in this section.

### 3.1. Field generation and flow computational method

Simulations were performed in four steps, consisting in the generation of the tested fields, simulation of flow, derivation of the flow lines and computation of the different indicators. The generation of the multi-Gaussian porous fields was performed via a Fourier transform [15] using the software FFTW [7,12]. Some fields are then rearranged according to the

rearrangement methods described in [43] and [20] if required. In order to avoid side effects, particularly with large correlation lengths, all fields were generated within a 1280x1280 grid of which the central part (128x128) was kept for the analysis, so $L$=128 was the characteristic system size. The original field was taken with a log-$k$ mean equal to zero, a variance ($\sigma_y^2$) equal to 1 and 3 and a correlation length ($\lambda$) equal to 8 and 64. Fracture networks were generated within a system size equal to $10*l_{min}$, where $l_{min}$ is the size of the smallest fracture.

In porous media, the flow equation was discretized on the structure of the medium according to a finite volume framework with harmonic inter-cell permeabilities [25]. As previously mentioned, permeameter-like boundary conditions were imposed on the sides of the domain, i.e. fixed heads on two opposite borders and no flow on the others. The discretized flow equations ended up to a linear system **A**.**x**=**b** solved by the multifrontal method implemented in the software UMFPACK [4]. Flow lines were constructed using a particle-tracking algorithm. Particles were injected through a vertical segment positioned in a central part at a distance of one correlation length from the inlet and proportionally to flow in order to avoid boundary effects [1,36]. Indicators were computed from 500 Monte-Carlo realizations for each tested case.

### 3.2. Description of the test cases

We used a broad range of 2D synthetic porous and fractured media characterized by the histogram of their permeability distribution and their connectivity structures. The synthetic porous media have all a lognormal permeability distribution of variance $\sigma_y^2$, where $y$ stands for log($k$) and $k$ is the permeability, but differ by their correlation structure (see Figure 2). For the same correlation length $\lambda$, we used six correlation patterns. The tested structures are identified by P as in porous and one or two other letters specifying the correlation pattern. The first two fields have Gaussian and exponential correlation structures (PG and PE in Figure 2).

231 The two next ones result from the rearrangement methods by *Zinn and Harvey* [43], yielding
232 fields of highly-connected high or low permeabilities (PC+ and PC- on Figure 2). The two last
233 ones are Gaussian-correlated fields to which are added highly permeable fracture-like
234 structures oriented parallel to the average head gradient and spanning either half of the system
235 (PF on Figure 2) or the whole system (PF2 on Figure 2) [20]. These rearrangement methods
236 provide different flow distributions (Figure 3). The C+ method increases the mean flow rate
237 compared to the Gaussian correlated field, while the F method adds a second peak of larger
238 flow rates to the histogram. Note, however, that the rearrangement methods do not modify the
239 permeability histogram.

240 Flow channeling was also observed in fractured media because of both the fractures and the
241 network-scale heterogeneities [38]. In this paper, we concentrated on the network-scale
242 complexity stemming at first from the power-law fracture length distribution:

$$n(l) \sim l^{-a} \tag{8}$$

243 where $a$ is a characteristic exponent between 1.5 and 4 [2]. We chose five types of fracture
244 networks differing by their fracture length and transmissivity distributions and by their
245 density. They are identified by the letter F followed by three additional letters. The first one,
246 FTL0, corresponds to fracture networks at percolation threshold (structures just connected)
247 with a power-law length distribution yielding to large fractures corresponding to $a$ equal to
248 2.0 (Figure 4). The four other networks show a smaller probability of occurrence of large
249 fractures ($a$=3.5) and are respectively at threshold (FTS0, Figure 4) and dense with a density
250 three times as large as that of threshold. The dense fracture networks differ by their fracture
251 transmissivity distributions of lognormal standard deviation $\sigma_y$ equal to 0 in FDS0, 1 in FDS1
252 and 2 in FDS2. Flow fields displayed in Figure 4 (second column) show different flow
253 structures from highly-channeled (FTL0, FTS0 and FDS2) to well-distributed (FDS0).

## 4. Results

After a visual inspection of the different test cases (Figure 2 and Figure 4), we ranked them by their apparent channeling degree (Table 2). The order was derived separately in the porous and fracture cases according to the flow-tube widths and regularity. In porous media, this order is consistent with $CF_1$ values (Table 3). All results discussed in the following paragraph are given in Table 3.

### 4.1. Relation between $D_{ic}$ and the number of considered flow tubes

The interchannel distance $D_{ic}$ (5) depends on the proportion of flow used to define a channel. If $n$ is the number of flow tubes, each flow tube carries $1/n$ part of the total flow. Figure 5 displays the relation between $D_{ic}$ and $1/n$. When $1/n$ tends to 1, $D_{ic}$ tends to $L$, meaning that no channel contains all the flow by itself. For the smallest values of $1/n$, the fracture cases reach a plateau characteristic of the smallest distance between flowing fractures. $1/n$ can be interpreted as characteristic of the smallest flow channel that can be identified. In Figure 5, we chose a value of $n$=20, for which all test cases have a characteristic interchannel distance larger than the interfracture distance. The value of $D_{ic}$ remains dependant of $n$ but the relative order for the different test cases remains the same whenever $n \leq 20$. We will thus compare $D_{ic}$ values between test cases rather than their absolute values in single test cases. The chosen value of $n$ is the flow-tube resolution. If $D_{ic} < L/n$, the medium will be considered as homogeneous in the sense that inter-channel distances are smaller than $L/n$. The value of $n$ should be increased for distinguishing closer channels.

### 4.2. Channeling characteristics $D_{ic}$ and $D_{cc}$

Figure 6a and Figure 6b display the two new indicators $D_{ic}/L$ and $D_{cc}/L'$ in highly-heterogeneous porous cases ($\sigma_y^2$=3) and fracture cases. PG and PE configurations have very close values of $D_{ic}$ and $D_{cc}$ despite the visual ranking, meaning that the short-range

correlations do not affect the channeling degree. Figure 6c and Figure 6d display the two other indicators $CF_1$ and $CT_1$. $CT_1$ performs poorly while $CF_1$ captures the channeling increase of porous configurations (PC+, PF and PF2). However, $CF_1$ can be used in porous cases but is not available in fractured media. Moreover, $CT_1$ is not discriminating in porous cases and does not account for the apparent ranking of channeling in the fracture test cases. $D_{ic}/L$ and $D_{cc}/L'$ are thus more adapted to characterize channeling consistently in porous and fractured cases.

The characteristic interchannel distance $D_{ic}/L$ consistently increases with more visual channeling. This increase is much smaller in the porous cases than in the fracture cases. $D_{cc}/L'$ also increases in porous media and has significantly larger values in all channeled fracture and porous fracture cases (FDS1, FDS2, FTL0, PF and PF2). In fact, in fractured media, flow is focused within the fractures and the variations of flow rates are more restricted than in porous media. $D_{cc}/L'$ reaches values close to one equivalent to little variation of flow rates within flow lines in FTL0, FDS2, PF and PF2. The comparison of the variations in $D_{ic}/L$ and $D_{cc}/L'$ shows that in the porous cases, $D_{cc}/L'$ increases over a range twice as large as that of $D_{ic}/L$ from PC- to PC+. In the fracture case, however, $D_{ic}/L$ is more consistent with the visual ranking of channeling than $D_{cc}/L'$. These results indicate that a flow organization indicator ($D_{cc}$) better characterizes porous flow channeling while a flow localization indicator ($D_{ic}$) better characterizes fracture flow channeling.

The variability of $D_{ic}$/L is much larger in fractured media than in porous media (Error bars in Figure 6a), which means that $D_{ic}$ does not vary much in porous configurations where channels are distributed over the field. However, $D_{ic}$ is highly variable in fracture configurations where channels can be either very clustered or spread.

The absence of systematic correlation between $D_{ic}/L$ and $D_{cc}/L'$ shown in Figure 7 confirms that $D_{ic}/L$ and $D_{cc}/L'$ characterize two different channeling properties. Figure 7 also shows that $D_{ic}/L$ and $D_{cc}/L'$ consistently characterize channeling in respectively the fracture and the porous cases. First, the visually ranked non-channeled fracture case FDS0 is in fact close to a highly-correlated porous case (PC+, $\sigma_y$=3, $\lambda$=8). Second, the porous fracture cases PF and PF2 located at the top left corner of Figure 7 have larger $D_{cc}/L'$ values than the porous cases and smaller $D_{cc}/L'$ values than the fracture channeled cases.

Based on Figure 7, we distinguish three types of flow structures. First, weakly-channeled flow structures are characteristic of Multi-Gaussian fields (PG, PE and PC-) and lead to small $D_{ic}/L$ and $D_{cc}/L'$ values. Second, the mildly-channeled flow structures were obtained for high-$k$ connected patterns (PC+, PF and PF2 with $\sigma_y^2$=1) and have small $D_{ic}/L$ values and large $D_{cc}/L'$ values. Third, the highly-channeled media have large $D_{ic}/L$ and $D_{cc}/L'$ values, like FTL0 or PF2 with $\sigma_y^2$=3. The latter case corresponds to extreme channeling for which flow is both highly localized and highly continuous in a very small number of channels.

### 4.3. Relation between channeling characteristics and *k*-field parameters

In this section, we look for a finer understanding of indicators $D_{ic}/L$ and $D_{cc}/L'$ by analyzing their dependence on the structures of the porous (Figure 8-9) and fractured test cases (Figure 10-12). We then comment on the variation trends and amplitudes. $D_{ic}/L$ systematically increases with more heterogeneity. In fact, $D_{ic}/L$ increases with $\sigma^2$ in porous media (Figure 8) and with $\sigma_y^2$ in fracture networks (Figure 12). Larger $\sigma^2$ values imply that flows focus in sparser transmissivity zones. $D_{ic}/L$ also systematically decreases in denser fracture networks, i.e. when increasing the number of connected parallel fracture paths (Figure 11). Increasing the probability of occurrence of long fractures with smaller $a$ values yields similar causes and effects (Figure 10). Similarly, increasing the correlation length $\lambda$ in porous media from small

to median values induces more channeling. The sole non-obvious $D_{ic}/L$ variation is its decrease from intermediary to large correlation lengths, approximately from $\lambda \sim L/8$ to $\lambda = L/2$ (Figure 9). This may be due to two reasons. First, the standard deviation of $D_{ic}/L$ steeply increases with $\lambda$ to the point where its variations become smaller than its variability. Second, when the large correlation length $\lambda$ is comparable to the system size $L$, for example for $\lambda = L/2$, the system becomes more homogeneous and channels are more regularly distributed, explaining the smaller value of $D_{ic}/L$. Apart from these side effects, $D_{ic}/L$ is first determined by the density of potential channels given by the correlation length in porous media and by fracture density and length distributions. Among the potential channels, only those made up of the higher permeabilities lead to effective channels. This is confirmed by the variation ranges of $D_{ic}/L$ presented in Table 4. The largest variation ranges are due to the fracture density first and to the difference of $D_{ic}/L$ values between porous and fracture cases (Figure 6). They cover at least two thirds of the full variation of $D_{ic}/L$. The variation ranges according to $\sigma_y^2$ are smaller but not negligible and account on average for less than half of the full variation range of porous and fracture cases.

$D_{cc}/L'$ is less variable than $D_{ic}/L$. It varies significantly only in PF as a function of $\sigma^2$ (Figure 8), in FDS as a function of $\sigma_y^2$ (Figure 12), in PG as a function of $\lambda$ (Figure 9) and in FD0 as a function of $a$ (Figure 10). We argue in the following that the sole genuine variation is the last one. The two first variations are due to the transition from porous to fractured cases. Beyond the transition ($\sigma_y^2 > 1$), $D_{cc}/L'$ is almost constant. In porous-fracture fields, small $\sigma^2$ values correspond to almost pure porous cases without fractures whereas high $\sigma^2$ values lead to fracture-like cases. In dense fracture networks with $\sigma_y^2 = 0$, the fracture network looks like a porous medium. Increasing $\sigma_y^2$ triggers channeling while keeping $D_{cc}/L'$ almost constant. $D_{cc}/L'$ decreases with the correlation length. This counter-intuitive result is only apparent and

mostly due to the simultaneous variations of $L$ and $\lambda$ in our simulation settings. In fact, we have found that $D_{cc}/L$' depends more on $L/\lambda$ than on $\lambda$. The range of variations of $D_{cc}/L$' is reduced from 0.25 to 0.09 when decreasing the range of variations of $L/\lambda$ from 64 to 8. Disregarding these dummy variations, the sole genuine variation that is not a transition is the increase in $D_{cc}/L$' with smaller $a$ values for dense networks (FD0). What fundamentally changes in the latter case is the nature of the correlations. $D_{cc}/L$' seems to be more affected by the nature of the correlation than by the variability of permeability. Aside from the large variation ranges due to a transition from porous-like to fracture-like media marked in grey in Table 4, it is the sole case where the variation range of $D_{cc}/L$' is significant. More precisely, it is of the order of three quarters of the full range of variations in all fracture networks, where all other cases are restricted to one quarter. The channel continuity measured by $D_{cc}/L$' is thus much more influenced by the nature of the correlation structure than by the other parameters including the permeability variability, the fracture density and the correlation length. $D_{cc}/L$' can be considered as an indicator of the nature of correlation. Finally, the absence of correlation between variability and $D_{cc}/L$' expresses that there is a fundamental limit in channeling related to the local permeability structure rather than to the permeability variability.

## 5. Discussion

As concluded in the previous section, the $D_{cc}/L$' ratio depends much more on the nature of the correlation than on the other parameters. The continuity of channels is at first a function of the occurrence of underlying-connected permeability structures. $D_{ic}/L$ is more intuitively a function of the density of paths and of the selection of the highest permeability paths.

Although $D_{ic}/L$ and $D_{cc}/L'$ have been defined as statistical characteristics, they are still rough estimates of the geometrical characteristics of the fields as shown in Figure 2. We recall that

373 $D_{ic}$ has been computed with a separation of flow tubes into 20 parts and thus measures
374 statistical properties of structures carrying at least 1/20 of the total flow. $D_{ic}$ is only slightly
375 variable for porous media and gives a characteristic scale of the low-flow zones (blue
376 patches). In simple multiGaussian cases (PG), $D_{ic}$ is close to the correlation length of the
377 velocity field. $D_{ic}$ is much more variable in the fracture networks where it is not too far from
378 the distance between effectively flowing structures. On the other hand, $D_{cc}$ is more variable in
379 the porous media than in the fracture networks. In the porous media, it gives a characteristic
380 scale of the extension of the high-flow zones (red flow tubes in Figure 2) and in fractured
381 media, it gives a characteristic length of flow channels.

382 As displayed in Figure 7, $D_{cc}/L'$ and $D_{ic}/L$ are not strongly correlated. Their dependences on
383 the different model parameters (Figure 8 to Figure 12) explain the lack of strong correlation.
384 Consequently, $D_{ic}$ and $D_{cc}$ actually do measure two different channeling characteristics that
385 are only weakly interdependent. In other words, they complementarily characterize
386 channeling.

387

388 Figure 13 displays the relation between the new indicators $D_{ic}/L$ and $D_{cc}/L'$ and the existing
389 indicators $CF_1$ and $CT_1$ [20]. $CT_1$ does not systematically identify the sparse fracture cases
390 (FTS0 and FTL0). Furthermore, $CT_1$ values within a single case are highly variable in
391 channeled media (Figure 14). $CT_1$ is thus not a good channeling indicator. The correlation of
392 $CF_1$ with $D_{cc}/L'$ is apparently better than with $D_{ic}/L$. $D_{cc}/L' < 0.5$ corresponds to weakly
393 negative $CF_1$ values, indicating flow fields slightly more influenced by low-permeability
394 zones. $D_{cc}/L' > 0.5$ corresponds to positive $CF_1$ values indicating flow fields more influenced
395 by the high- permeability zones making up the channels. The advantage of $D_{cc}/L'$ over $CF_1$ is
396 that the correlation structures are better distinguished. For example, PC+ and PF have very

close $CF_1$ values (Figure 6) but differ by their $D_{cc}/L'$ values. This difference stems from the more contrasted channels in the PF configuration relative to the PC+ configuration, despite the similar channeling intensity. However, it must be noted that $CF_1$ better distinguish PF from PF2 than $D_{ic}/L$ and $D_{cc}/L$. The second advantage of $D_{cc}/L'$ over $CF_1$ is that it provides information on the flow structure in both porous and fracture cases

$D_{ic}/L$ and $D_{cc}/L'$ could also be readily computed in anisotropic and 3D fields. We expect both anisotropy and 3D to increase $D_{cc}/L'$ without significantly modifying $D_{ic}/L$. $D_{ic}/L$ will remain linked to the volume of the low-flow zones, the characteristic size of which will not be strongly modified. However, we expect anisotropy to increase $D_{cc}/L'$ just by the effect of the higher velocity correlations in the flow direction. 3D could also potentially provide longer and more tortuous channels around the low-flow zones, and hence increase $D_{cc}/L'$.

The derivation of $D_{ic}/L$ and $D_{cc}/L'$ in natural cases is more difficult because of the lack of data that would lead to their direct estimate. They could however be inferred from the geometrical and hydraulic characteristics of the permeability field either with the results of this study or with closer simulations. It would be interesting, in field cases, to condition the estimation of these indexes on permeability and flow values and thus to lower the non-negligible variability displayed in Figure 14.

## 6. Summary and Conclusion

Channeling has been observed both in field and in synthetic contexts. However, its characterization has been essentially qualitative. We introduce two statistical indicators based on the distribution of flow rates and compute them on a wide variety of porous and fracture permeability fields. The tested fields range, in porous media, from multi-Gaussian fields with classical correlation laws (Gaussian and exponential) to permeability fields rearranged to enhance channeling using the method by *Zinn and Harvey* and to permeability fields

rearranged to mimic the presence of fractures within the field. The tested fractured media cover a broad range of fracture lengths, densities and transmissivity distributions.

The first indicator, $D_{ic}$, is related to the characteristic interchannel distance. It is based on the participation ratio $S_2$ applied to the distribution of flow-tube widths. Although statistically derived, this ratio can be interpreted as a characteristic scale of the low-flow zones perpendicular to the flow. It is moreover highly sensitive to the variability of the permeability, as well as to the permeability correlation pattern. The second indicator, $D_{cc}$, is related to a characteristic extension of channels. It is too computed with the participation ratio $S_2$ applied to the Lagrangian derivative distribution of flow rates. It is highly sensitive to the nature of the permeability correlation structure, which is also an important channeling cause. Both indicators consistently characterize flow channeling in porous and fractured media, with $D_{ic}$ being more sensitive in fractured media and $D_{cc}$ in porous media. As they are weakly correlated, they measure different channeling characteristics that are weakly dependent and are complementary to characterize channeling in porous and in fractured media. As a result, they are complementary to identify and quantify channeling in various media, from non-channeled fields like multi-Gaussian permeability fields with common correlation laws to highly-channeled media like porous-fractured fields with a large variability and fracture network with large fractures and broadly distributed transmissivity values. We will use the proposed indicators in further studies to distinguish weakly-, mildly- and highly-channeled media in order to choose the most relevant modeling framework and identification strategies.

**Acknowledgements**

The French National Research Agency ANR is acknowledged for its financial founding through the MOHINI project (ANR-07-VULN-008) and for its contribution to the

development of numerical methods through the MICAS project (ANR-07-CIS7-004). The authors thank two anonymous reviewers for their highly detailed and constructive reviews.

[1] A. Beaudoin, J.-R. de Dreuzy, and J. Erhel, An Efficient Parallel Particle Tracker for Advection-Diffusion Simulations in Heterogeneous Porous Media in: Springer, (Ed.), Euro-Par 2007 Parallel Processing, Berlin / Heidelberg, 2007.
[2] E. Bonnet, O. Bour, N.E. Odling, P. Davy, I. Main, P. Cowie, and B. Berkowitz, Scaling of fracture systems in geological media. Reviews of Geophyics 39 (2001) 347-383.
[3] C. Bruderer-Weng, P. Cowie, Y. Bernabé, and I. Main, Relating flow channelling to tracer dispersion in heterogeneous networks. Adv. Water Resources 27 (2004) 843-855.
[4] T.A. Davis, Algorithm 832: UMFPACK, an unsymmetric-pattern multifrontal method. ACM transactions on Mathematical Software 30 (2004) 196-199.
[5] P. Davy, A. Hansen, E. Bonnet, and S.-Z. Zhang, Localization and fault growth in layered brittle-ductible systems: Implications for deformations of the continental lithosphere. J. Geophys. Res. 100 (1995) 6281-6294.
[6] J.-R. de Dreuzy, P. Davy, and O. Bour, Hydraulic properties of two-dimensional random fracture networks following a power law length distribution 1. Effective connectivity. Water Resour. Res. 37 (2001) 2065–2078.
[7] J.R. de Dreuzy, A. Beaudoin, and J. Erhel, Asymptotic dispersion in 2D heterogeneous porous media determined by parallel numerical simulations. Water Resources Research 43 (2007) 13.
[8] G. de Marsily, F. Delay, J. Gonçalvès, P. Renard, V. Teles, and S. Violette, Dealing with spatial heterogeneity. Hydrogeology Journal 12 (2005) 161-183.
[9] A.J. Desbarats, Spatial Averaging of Hydraulic Conductivity in Three-Dimensional Heterogeneous Porous Media. Mathematical Geology 24 (1992) 249-267.
[10] G.E. Fogg, Groundwater flow and sand body interconnectedness in a thick, multiple aquifer system. Water Resources Research 22 (1986) 679-694.
[11] G.E. Fogg, S.F. Carle, and C. Green, Connected-network paradigm for the alluvial aquifer system. in: D. Zhang, and C.L. Winter, (Eds.), Theory, modeling and field investigation in hydrogeology: A special volume in honor of Shlomo P Neuman's 60th. birthday, Geological Society of America, 2000, pp. 25-42.
[12] M. Frigo, and S.G. Johnson, The design and implementation of FFTW3. Proceedings of the IEEE 93 (2005) 216-231.
[13] C.C. Frippiat, T.H. Illangasekare, and G.A. Zyvoloski, Anisotropic effective medium solutions of head and velocity variance to quantify flow connectivity. Advances in Water Resources 32 (2009) 239-249.
[14] A.J. Guswa, and D.L. Freyberg, On using the equivalent conductivity to characterize solute spreading in environments with low-permeability lenses. Water Resources Research 20 (2002).
[15] A.L. Gutjahr, Fast Fourier transforms for random field generation, New Mexico Tech project report 4-R58-2690R, 1989.
[16] J.S. Hanor, Effective hydraulic conductivity of fractured clay beds at a hazardous waste landfill; Louisiana Gulf Coast. Water Resources Research 29 (1993) 3691-3698.
[17] A. Journel, and F.G. Alabert, Focusing on spatial connectivity of extreme-valued attributes : stochastic indicator models of reservoir heterogeneities. AAPG Bulletin 73 (1989).
[18] A.G. Journel, C.V. Deutsch, A.J. Desbarats, and A. Stanford, Power Averaging for Block Effective Permeability, SPE California Regional Meeting, 2-4 April 1986, Soc. Petro. Eng. , Oakland, California, 1986.

494 [19] J. Kerrou, P. Renard, H.-J. Hendricks Franssen, and I. Lunati, Issues in characterizing
495 heterogeneity and connectivity in non-multiGaussian media. Advances in Water
496 Resources 31 (2008) 147-159.
497 [20] C. Knudby, and J. Carrera, On the relationship between indicators of geostatistical, flow
498 and transport connectivity. Adv. Water Resources 28 (2005) 405-421.
499 [21] C. Knudby, and J. Carrera, On the use of apparent hydraulic diffusivity as an indicator of
500 connectivity. Journal of Hydrology 329 (2006) 377-389.
501 [22] C. Knudby, J. Carrera, J.D. Bumgardner, and G.E. Fogg, Binary upscaling - the role of
502 connectivity and a new formula. Adv. Water Resources 29 (2006).
503 [23] C.E. Koltermann, and S.M. Gorelick, Heterogeneity in sedimentary deposits: a review of
504 structure imitating, process-imitating and descriptives approaches. Water Resources
505 Research 32 (1996) 2617-2658.
506 [24] S. Krishnan, and A. Journel, Spatial connectivity : from variograms to multiple-point
507 measures. Mathematical Geology 35 (2003) 915-925.
508 [25] R. Kruel-Romeu, and B. Noetinger, Calculation of internodal transmissivities in finite
509 difference models of flow in heterogeneous porous media. Water Resources Research
510 31 (1995) 943-959.
511 [26] T. Le Borgne, J.R. de Dreuzy, P. Davy, and O. Bour, Characterization of the velocity
512 field organization in heterogeneous media by conditional correlation. Water Resources
513 Research 43 (2007) 10.
514 [27] G. Matheron, Elements pour une théorie des milieux poreux, Masson et Cie, 1967.
515 [28] L. Moreno, and C.F. Tsang, Flow channeling in strongly heterogeneous porous media.
516 Water Resources Research 30 (1994) 1421-1430.
517 [29] C.-H. Park, C. Beyer, S. Bauer, and O. Kolditz, A study of preferential flow in
518 heterogeneous media using random-walk particle tracking. Geosciences Journal 12
519 (2008).
520 [30] M.J. Ronayne, and S.M. Gorelick, Effective permeability of porous media containing
521 branching channel networks. Physical Review E 73 (2006).
522 [31] M.J. Ronayne, S.M. Gorelick, and J. Caers, Identifying discrete geologic structures that
523 produce anomalous hydraulic response: an inverse modeling approach. Water
524 Resources Research 44 (2008).
525 [32] X. Sánchez-Vila, J. Carrera, and J.P. Girardi, Scale effects in transmissivity. Journal of
526 Hydrology 183 (1996) 1-22.
527 [33] T. Scheibe, and S. Yabusaki, Scaling of flow and transport behavior in heterogeneous
528 groundwater systems. Advances in Water Resources 22 (1998) 223-238.
529 [34] S.E. Silliman, An interpretation of the difference between aperture estimates derived
530 from hydraulic and tracer tests in a single fracture. Water Resources Research 25
531 (1989) 2275-2283.
532 [35] A. Sornette, P. Davy, and D. Sornette, Fault Growth in Brittle-Ductile Experiments and
533 the Mechanics of Continental Collisions. J. Geophys. Res. 98 (1993) 12,111.
534 [36] A.F.B. Tompson, and L.W. Gelhar, Numerical-simulation of solute transport in 3-
535 dimensional, randomly heterogeneous porous-media. Water Resources Research 26
536 (1990) 2541-2562.
537 [37] P. Trinchero, X. Sánchez-Vila, and D. Fernàndez-Garcia, Point-to-point connectivity, an
538 abstract concept or a key issue for risk assessment studies? Adv. Water Resources 31
539 (2008) 1742-1753.
540 [38] C.-F. Tsang, and I. Neretnieks, Flow Channeling in heterogeneous fractured rocks.
541 Reviews of Geophyics 36 (1998).

[39] Y.W. Tsang, and C.F. Tsang, Flow channeling in a single fracture as a two dimensional strongly heterogeneous permeable medium. Water Resources Research 25 (1989) 2076-2080.
[40] J.E. Warren, and H.H. Price, Flow in heterogeneous porous media. Soc. Petr. Eng 1 (1961) 153-169.
[41] X.-H. Wen, and J.J. Gomez-Hernandez, Numerical modeling of macrodispersion in heterogeneous media - a comparison of multi-Gaussian and non-multi-Gaussian models. J cont hydrol 30 (1998) 129-156.
[42] A.W. Western, G. Blöschl, and R.B. Grayson, Toward capturing hydrologically significant connectivity in spatial patterns. Water Resources Research 37 (2001) 83-97.
[43] B. Zinn, and C.F. Harvey, When good statistical models of aquifer heterogeneity go bad: a comparison of flow, dispertion and mass transfer in connected and multivariate Gaussian hydraulic conductivity fields. Water Resources Research 39 (2003).

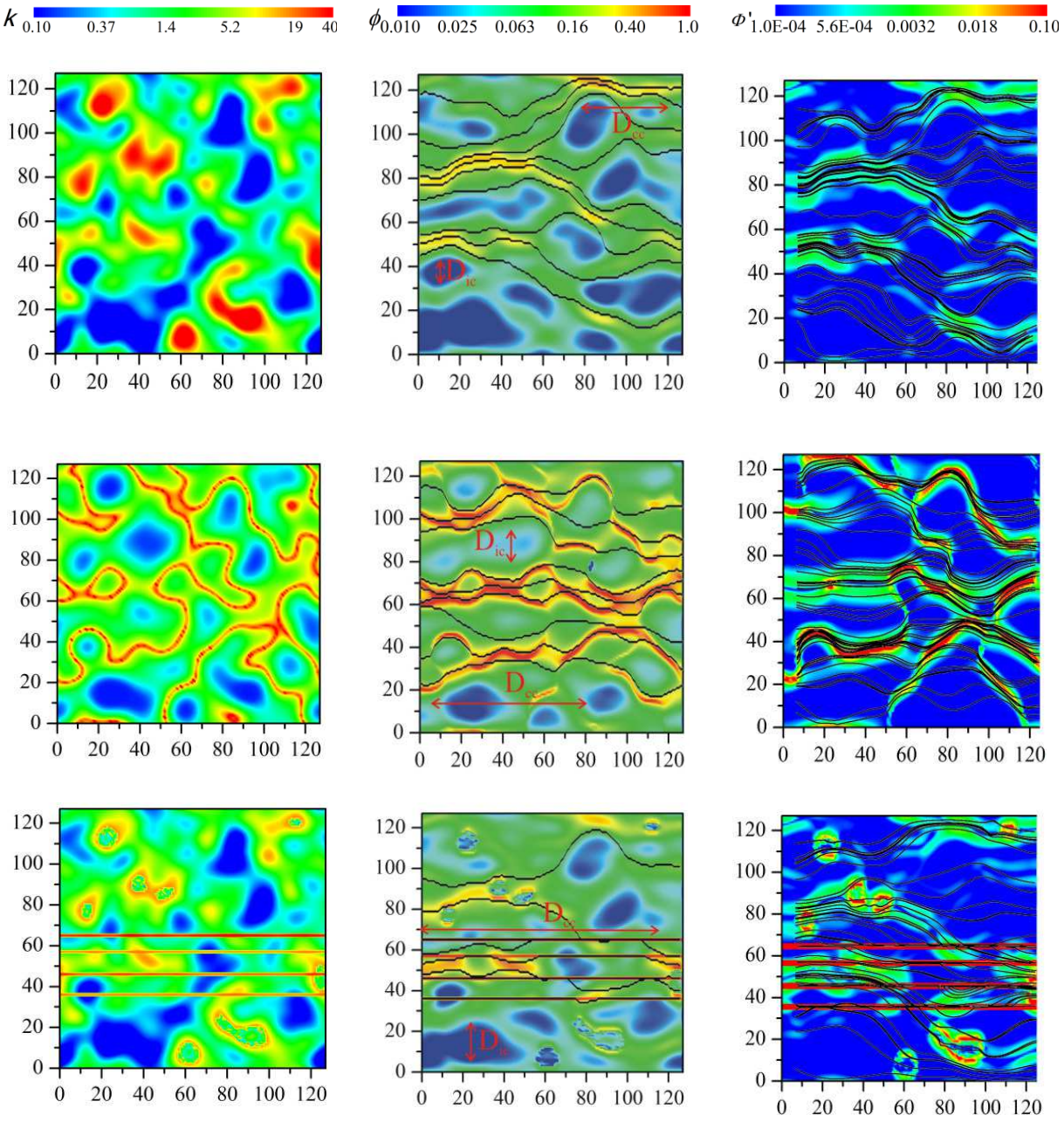


559 Figure 1: Permeability fields $K$ (left), flow rates $\phi$ (middle) and Lagrangian derivatives of
560 flow rates $\phi'$ (right) in three permeability fields, all based on the same multi-Gaussian
561 distribution with a Gaussian correlation. The correlation length is fixed to 1/16$^{th}$ of the system
562 size. Correlations are either not modified (top) or increased either by connecting the larger
563 permeability values (middle) [43] or by introducing fracture-like structures (bottom) [20]. 10
564 flow tubes as well as the $D_{ic}$ and $D_{cc}$ values defined in section 2 are superimposed on the

565 fields of the middle column. 50 flow lines are superimposed on the distribution values of

566 Lagrangian flow derivatives of the right column.

| Test case | Conductivity field | Flow field |
|---|---|---|
| **PC-** | 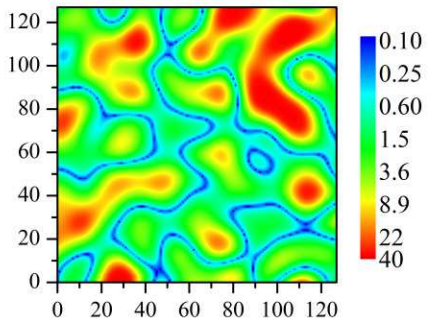 | 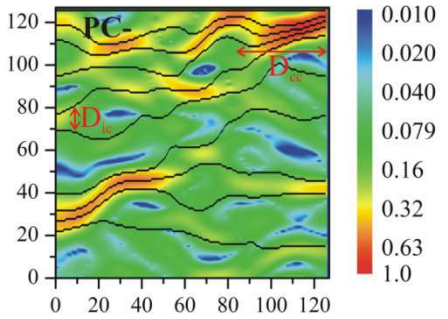 |
| **PG** | 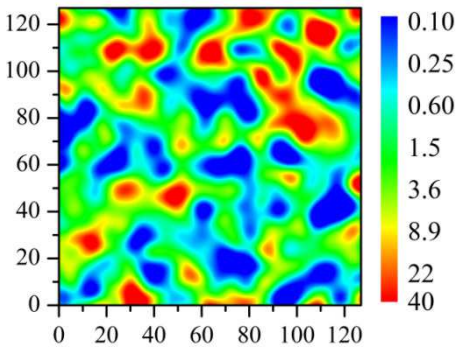 | 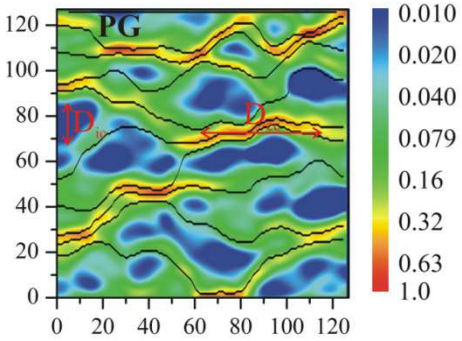 |
| **PE** | 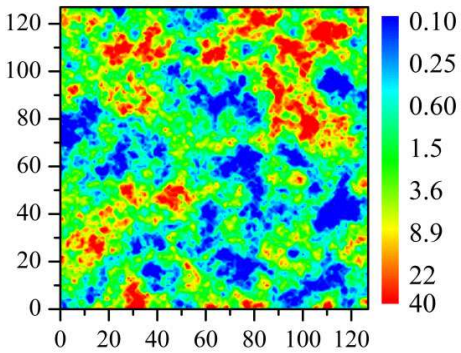 | 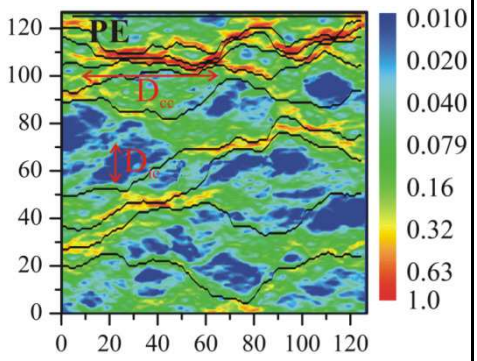 |

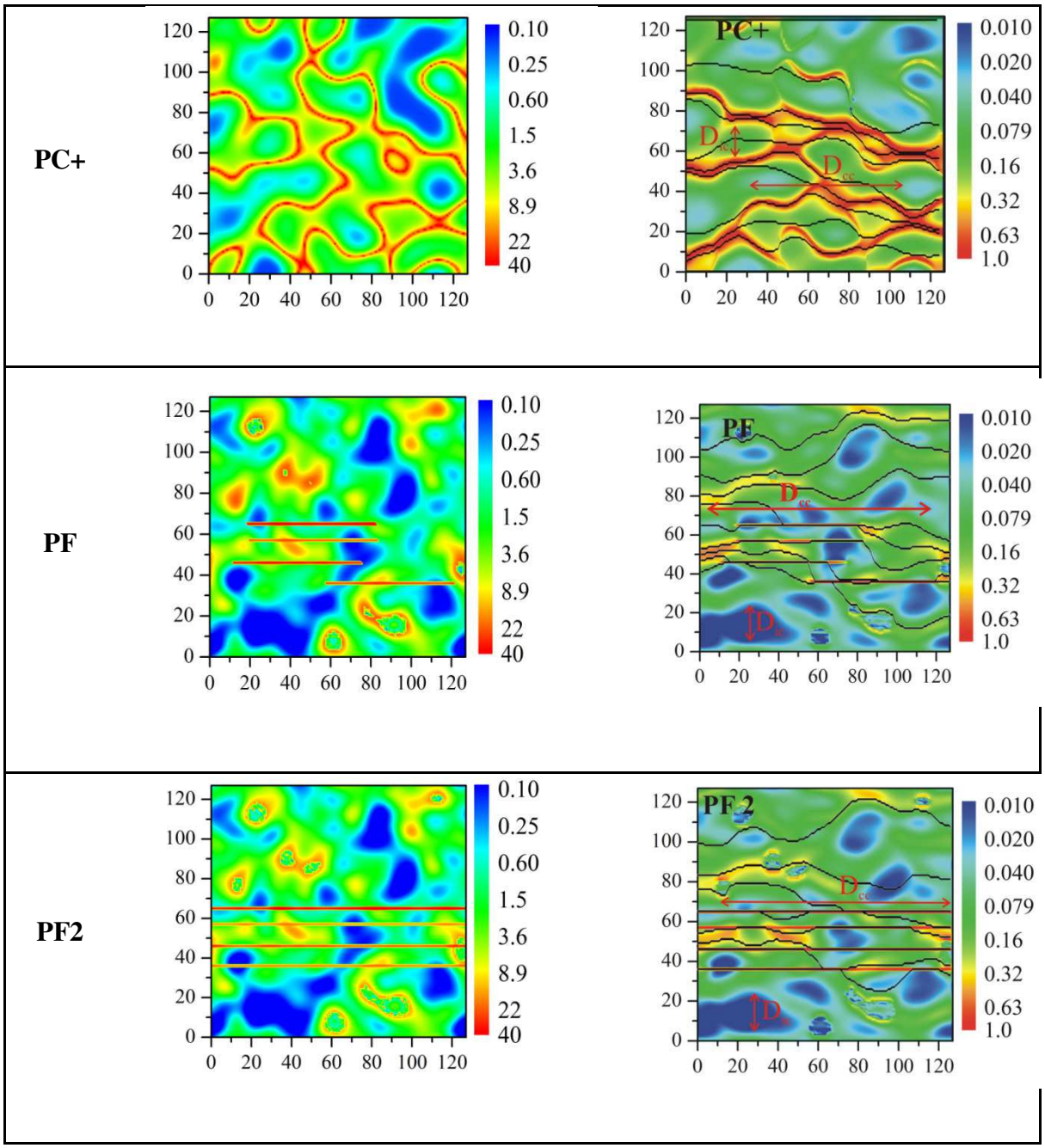


Figure 2: Permeability fields (left) associated with their corresponding flow fields (right). Permeabilities are normalized by their geometrical mean value. Flows are normalized by their maximal value. Test case names in the first column refer to Table 2. $D_{ic}$ and $D_{cc}$ values defined in section 2 are superimposed on the flow fields of the right column.

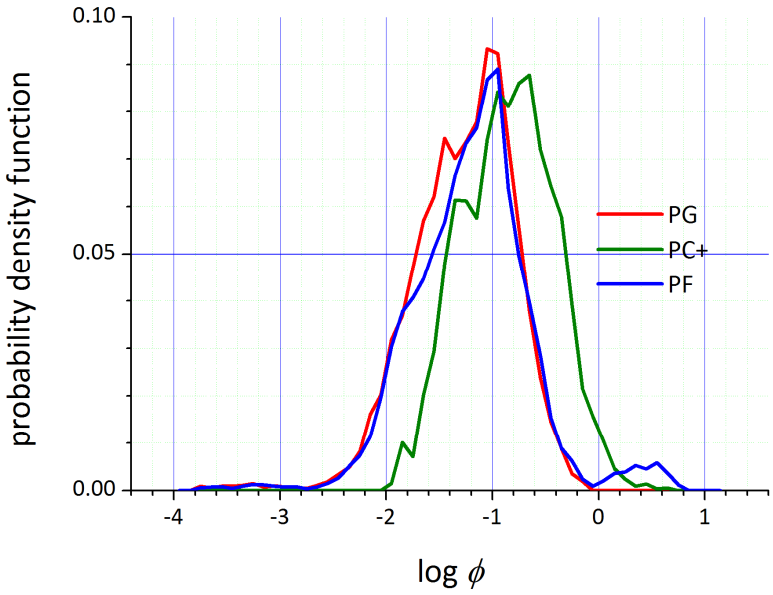


572

573 Figure 3: Probability density function of the logarithm of flow rates in the classical multi-
574 Gaussian fields with a Gaussian correlation (PG) and in the fields with the two rearrangement
575 methods PC+ and PF. The C+ rearrangement method globally shifts the flow rate distribution
576 to higher flow values while the F rearrangement introduces a second peak of higher flow
577 values.

578

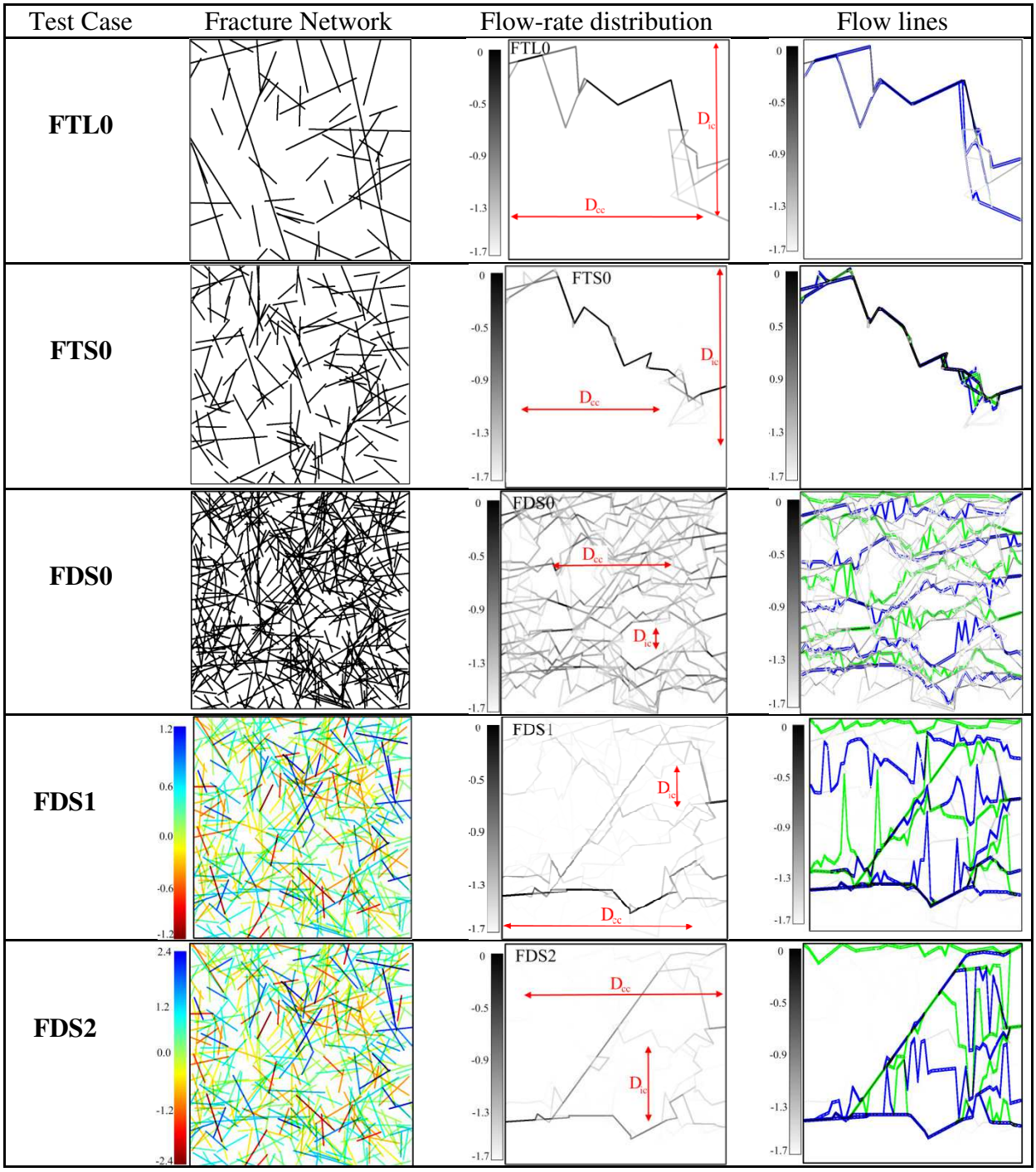


Figure 4: (Left) Fracture test cases, colored according to their log-transmissivity (middle) corresponding flow fields with $D_{ic}$ and $D_{cc}$ and (right) flow tubes. Flows are normalized by their maximal value and colored with a logarithmic scale. Test case names in the first column refer to Table 2.

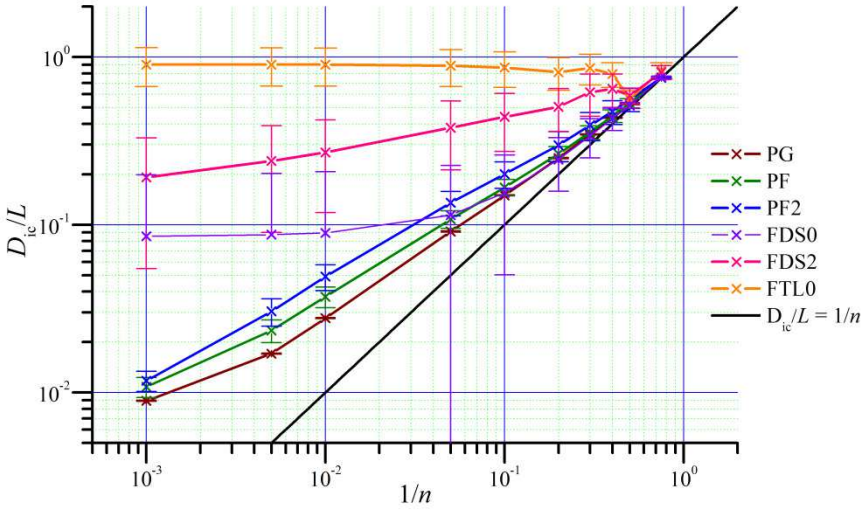


585

586 Figure 5: $D_{ic}/L$ versus $1/n$ in various porous and fractured test cases. The vertical black line
587 represents the values used in the current study. $D_{ic}/L=1/n$ is the lower limit representing a
588 homogeneous field while $D_{ic}/L=1$ is the upper limit representing a field with all flows
589 concentrated in a unique channel.

590

591

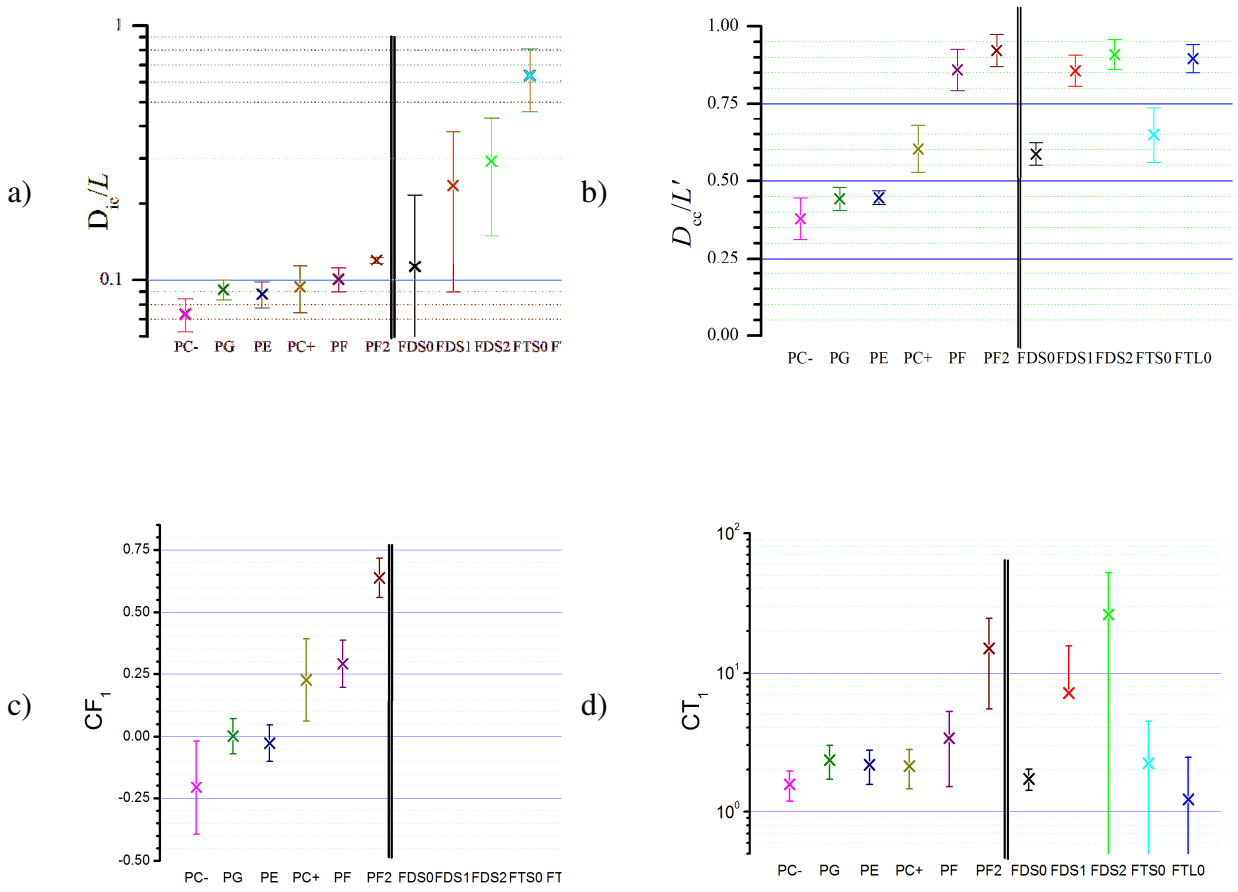


592 Figure 6: Values of (a) $D_{ic}$/L, (b) $D_{cc}/L'$, (c) $CF_1$ and (d) $CT_1$. For the different test cases
593 ranked by their increasing intuitive rating of channeling (Table 2), Error bars are the standard
594 deviations of the underlying distributions. Parameters of porous cases are $\sigma_y^2$=3 and $\lambda$=8. The
595 vertical double bar separates porous and fracture test cases.

596

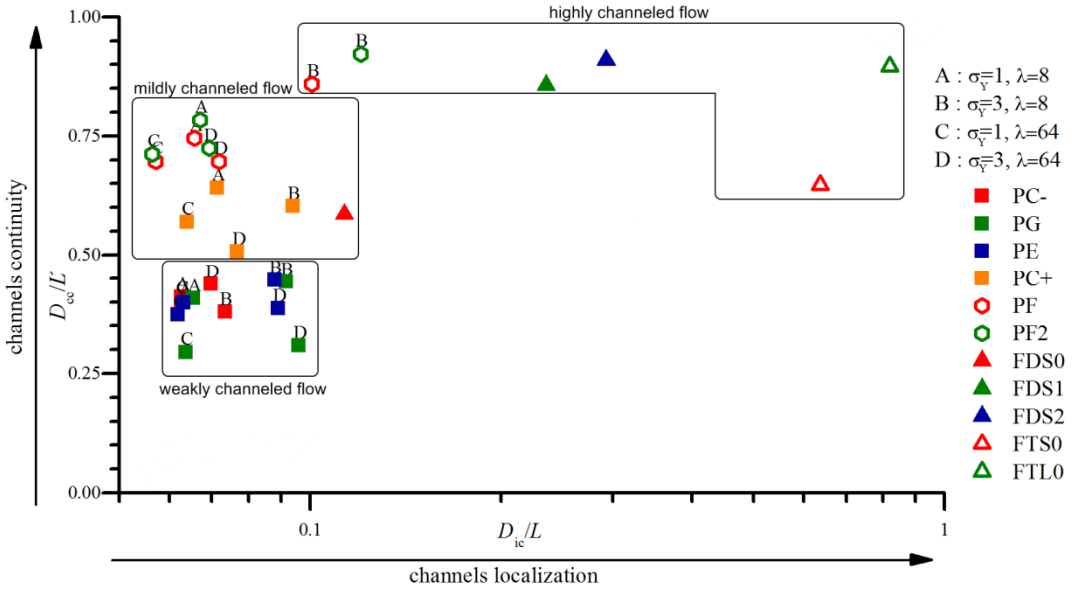


597

598 Figure 7: $D_{ic}/L$ versus $D_{cc}/L'$ in porous and fractured fields. Porous cases are represented by
599 squares, fractured cases by triangles and porous fractured cases by hexagons. The
600 combination of the two indicators give an estimation of the channeling degree with weakly-
601 channeled configurations (small $D_{ic}$, small $D_{cc}$), mildly-channeled configurations (high $D_{cc}$,
602 small $D_{ic}$) and highly-channeled configurations (high $D_{ic}$, high $D_{cc}$).

603

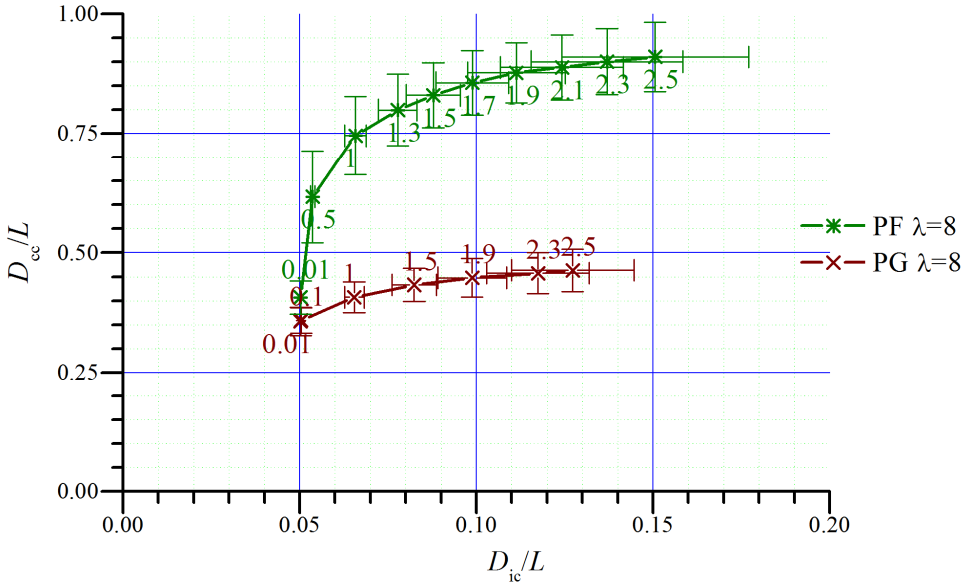


604

605 Figure 8: Variation of $D_{cc}/L'$ versus $D_{ic}/L$ in porous test cases PG and PF for varying
606 permeability standard deviations $\sigma_y$. $\sigma_y$ values are given next to the corresponding symbols.
607 When $\sigma_y$ tends to zero, $D_{ic}$ tends to $1/n$ and $D_{cc}$ tends to zero as the permeability values tend
608 to be homogeneous.

609

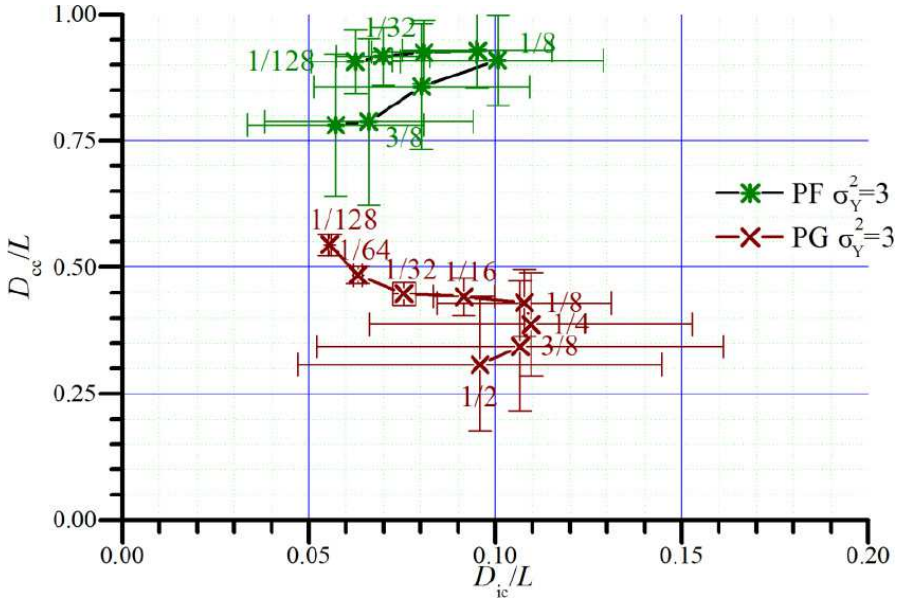


610

611 Figure 9: Variation of $D_{cc}/L'$ versus $D_{ic}/L$ in porous test cases PG and PF for varying

612 permeability correlation lengths $\lambda$. $\lambda$ values are given next to the corresponding symbols.

613

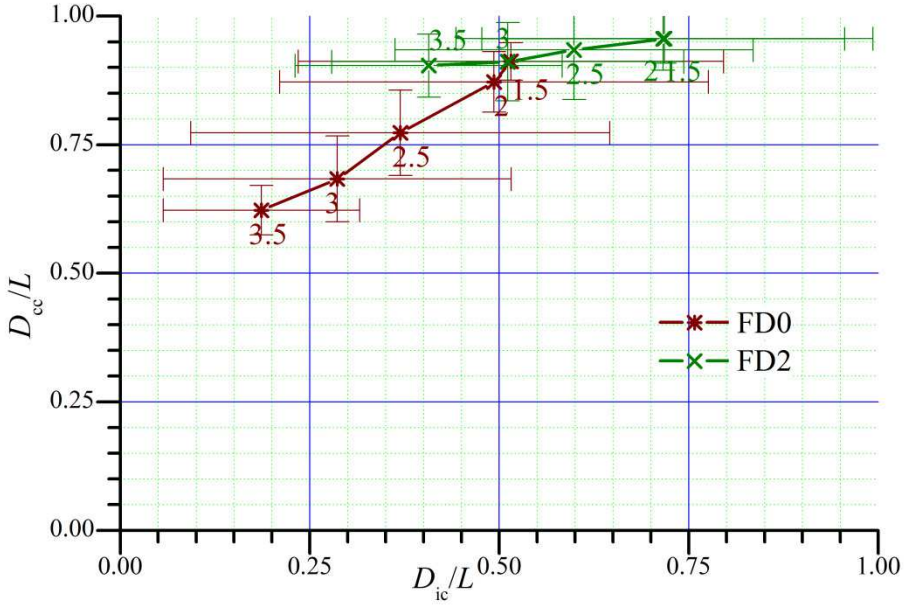


614

615 Figure 10: $D_{cc}/L'$ versus $D_{ic}/L$ in fractured test cases with varying power-law length

616 exponents $a$. Values of $a$ are given next to the corresponding symbols.

617

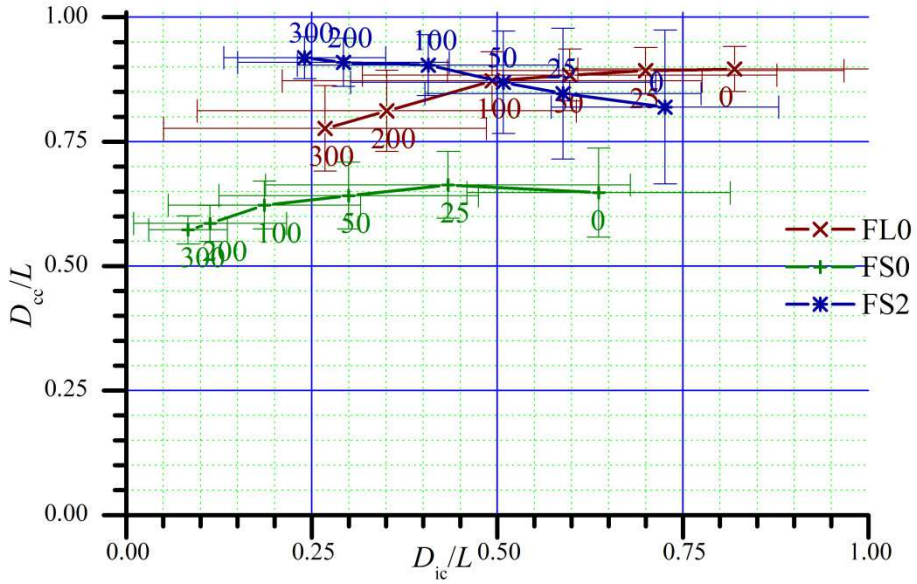


Figure 11: $D_{cc}/L'$ versus $D_{ic}/L$ in fractured test cases with varying fracture densities $d$. Values of $d$ are given next to the corresponding symbols. Density is measured as the percentage of fractures above percolation threshold. It is 0 at percolation threshold and 100 in networks having twice as much fractures as in networks at percolation threshold.

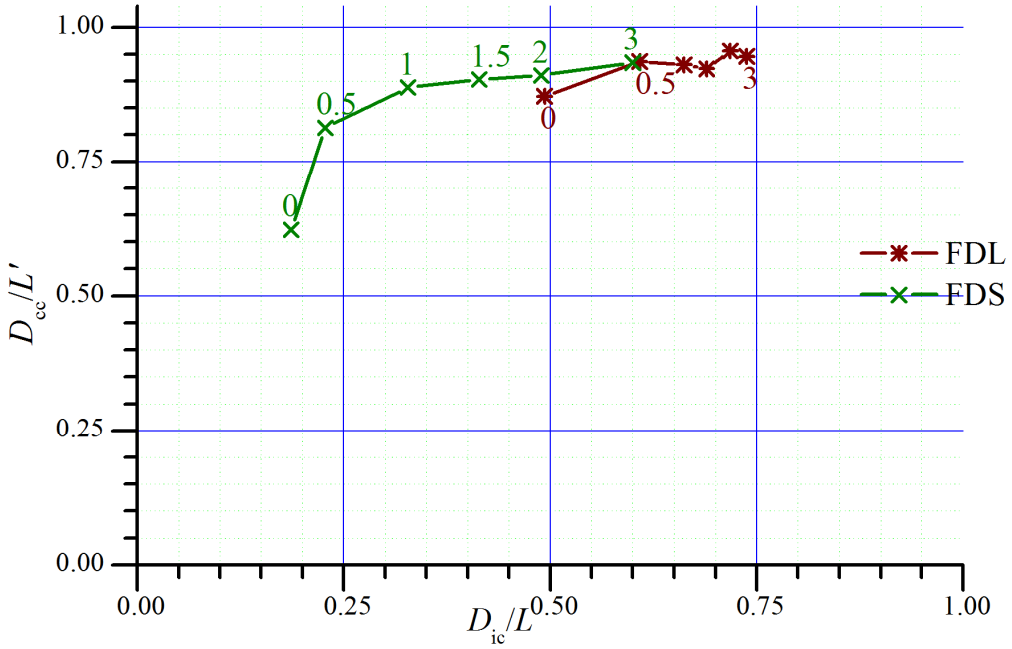


624

625 Figure 12: $D_{cc}/L'$ versus $D_{ic}/L$ in fractured test cases with varying variances of the

626 transmissivity distribution $\sigma_Y^2$. Values of $\sigma_Y^2$ are given next to the corresponding symbols.

627

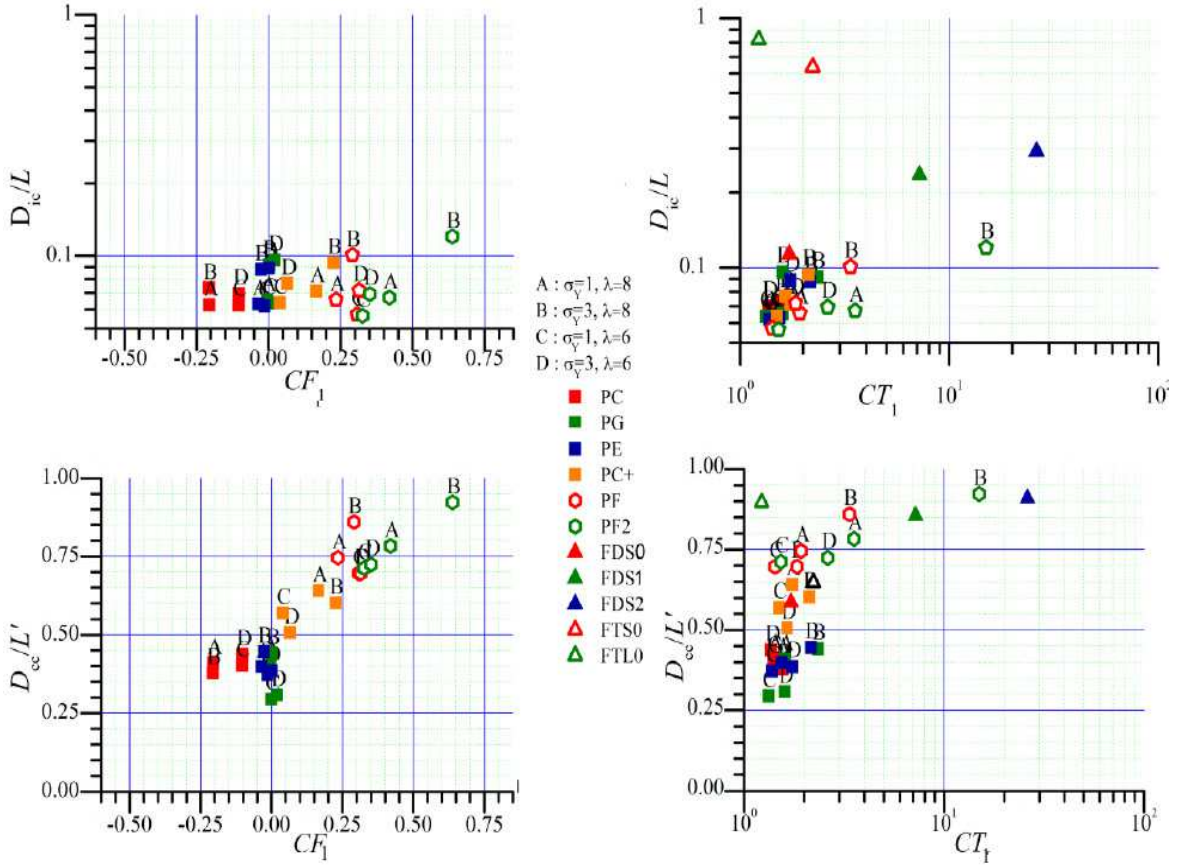


628

629 Figure 13: Channeling characteristics ($D_{ic}/L$ and $D_{cc}/L'$) versus indicators $CF_1$ and $CT_1$

630 defined in [20]. Note that $D_{ic}$ is available only in porous cases.

631

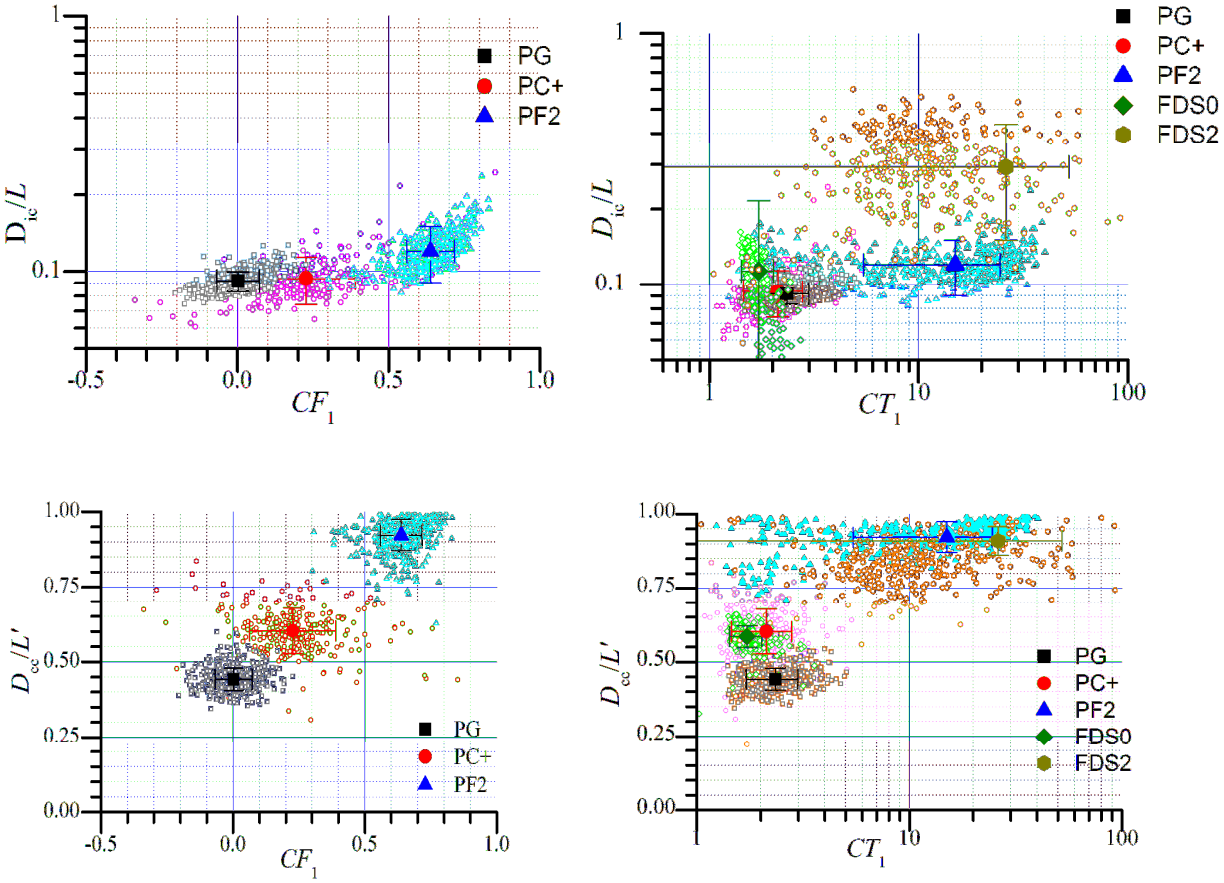


Figure 14: $D_{ic}/L$ and $D_{cc}/L'$ versus $CF_1$ and $CT_1$. This figure shows the variability of the indicators by depicting the 500 values for PG, PC+ and PF2 ($\sigma_y^2$=3, $\lambda$=8) and, if available, FDS0 and FDS2. Small points stand for the 500 results and large points for the associated mean. Error bars stand for the standard deviation. $D_{ic}$ and $D_{cc}$ are generally less variable in the same configurations than $CF_1$, and particularly than $CT_1$.

639

| Distribution type | Parameters | $S_2$ |
|---|---|---|
| Gaussian | mean $\mu$ and variance $\sigma_G$ | $S_2=(1+(\sigma_G/\mu)^2)^{-1}$ |
| Log-normal | log-normal variance $\sigma_{LN}^2$ | $S_2=\exp(-\sigma_{LN}^2)$ |
| Binary distribution | $v_1$ with a probability $p$ and 0 with a probability 1-$p$ | $S_2=p$ |

640 Table 1: Participation ratio $S_2$ for classical distributions.

641

642

| Field Type | Properties | Short name |
|---|---|---|
| Porous | Rearranged with the C- method, $\sigma_y^2$=1 or 3, $\lambda$=$L$/16 or $L$/2 | PC- |
| Porous | Gaussian correlation, $\sigma_y^2$=1 or 3, $\lambda$=$L$/16 or $L$/2 | PG |
| Porous | Exponential correlation, $\sigma_y^2$=1 or 3, $\lambda$=$L$/16 or $L$/2 | PE |
| Porous | Rearranged with the C+ method, $\sigma_y^2$=1 or 3, $\lambda$=$L$/16 or $L$/2 | PC+ |
| Porous | Rearranged with the F method, $\sigma_y^2$=1 or 3, $\lambda$=$L$/16 or $L$/2 | PF |
| Porous | Rearranged with the F2 method, $\sigma_y^2$=1 or 3, $\lambda$=$L$/16 or $L$/2 | PF2 |
| Fractured | Dense ($d$=3$p_c$), dominated by short fractures ($a$=3.5), uniform fracture transmissivity ($\sigma_y^2$=0) | FDS0 |
| Fractured | Dense ($d$=3$p_c$), dominated by short fractures ($a$=3.5), distributed fracture transmissivity ($\sigma_{y\,\log T}^2$=1) | FDS1 |
| Fractured | Dense ($d$=3$p_c$), dominated by short fractures ($a$=3.5), distributed fracture transmissivity ($\sigma_{y\,\log T}^2$=2) | FDS2 |
| Fractured | Sparse ($d$=$p_c$), dominated by short fractures ($a$=3.5), constant fracture transmissivity ($\sigma_{y\,\log T}^2$=0) | FTS0 |
| Fractured | Sparse ($d$=$p_c$), dominated by long fractures ($a$=2.0), constant fracture transmissivity ($\sigma_{y\,\log T}^2$=0) | FTL0 |

643 Table 2: Porous and fractured test cases ranked visually by increasing order of channeling.

| CASE | $\sigma_y^2$ | $\lambda$ | $D_{ic}/L$ | $\sigma^2$ ($D_{ic}/L$) | $D_{cc}/L'$ | $\sigma^2$ ($D_{cc}/L'$) | $CF_1$ | $\sigma^2$ ($CF_1$) | $CT_1$ | $\sigma^2$ ($CT_1$) |
|---|---|---|---|---|---|---|---|---|---|---|
| PC- | 1 | 8 | 0.063 | 0.0040 | 0.4 | 0.0820 | -0.20 | 0.17 | 1.4 | 0.22 |
| | 3 | | 0.073 | 0.011 | 0.38 | 0.066 | -0.21 | 0.19 | 1.6 | 0.38 |
| | 1 | 64 | 0.061 | 0.0080 | 0.40 | 0.18 | -0.10 | 0.50 | 1.4 | 0.35 |
| | 3 | | 0.070 | 0.022 | 0.44 | 0.20 | -0.10 | 0.51 | 1.4 | 0.34 |
| PG | 1 | 8 | 0.065 | 0.0027 | 0.41 | 0.032 | -0.0042 | 0.076 | 1.6 | 0.25 |
| | 3 | | 0.092 | 0.0082 | 0.44 | 0.037 | 0.0014 | 0.071 | 2.3 | 0.64 |
| | 1 | 64 | 0.064 | 0.014 | 0.29 | 0.088 | -0.00023 | 0.43 | 1.3 | 0.28 |
| | 3 | | 0.096 | 0.049 | 0.31 | 0.13 | 0.020 | 0.41 | 1.6 | 0.55 |
| PE | 1 | 8 | 0.063 | 0.0031 | 0.40 | 0.016 | -0.035 | 0.075 | 1.5 | 0.25 |
| | 3 | | 0.088 | 0.010 | 0.45 | 0.022 | -0.026 | 0.073 | 2.2 | 0.60 |
| | 1 | 64 | 0.062 | 0.0087 | 0.37 | 0.030 | -0.015 | 0.27 | 1.4 | 0.26 |
| | 3 | | 0.089 | 0.032 | 0.39 | 0.065 | 0.00018 | 0.26 | 1.7 | 0.55 |
| PC+ | 1 | 8 | 0.071 | 0.0064 | 0.64 | 0.066 | 0.17 | 0.15 | 1.7 | 0.42 |
| | 3 | | 0.094 | 0.020 | 0.60 | 0.075 | 0.23 | 0.16 | 2.1 | 0.67 |
| | 1 | 64 | 0.064 | 0.016 | 0.57 | 0.21 | 0.039 | 0.53 | 1.5 | 0.50 |
| | 3 | | 0.077 | 0.035 | 0.51 | 0.22 | 0.065 | 0.53 | 1.7 | 0.73 |
| PF | 1 | 8 | 0.066 | 0.0030 | 0.74 | 0.082 | 0.23 | 0.12 | 1.9 | 0.54 |
| | 3 | | 0.10 | 0.011 | 0.86 | 0.067 | 0.29 | 0.09 | 3.4 | 1.8 |
| | 1 | 64 | 0.057 | 0.0053 | 0.70 | 0.12 | 0.31 | 0.31 | 1.4 | 0.25 |
| | 3 | | 0.071 | 0.017 | 0.70 | 0.15 | 0.31 | 0.31 | 1.8 | 0.68 |
| PF2 | 1 | 8 | 0.067 | 0.0037 | 0.78 | 0.076 | 0.42 | 0.12 | 3.5 | 2.4 |
| | 3 | | 0.12 | 0.0030 | 0.92 | 0.052 | 0.64 | 0.078 | 15 | 9.6 |
| | 1 | 64 | 0.056 | 0.060 | 0.71 | 0.11 | 0.33 | 0.32 | 1.5 | 0.55 |
| | 3 | | 0.069 | 0.1861 | 0.72 | 0.14 | 0.35 | 0.33 | 2.6 | 2.6 |
| FDS0 | N/A | | 0.11 | 0.10 | 0.59 | 0.036 | N/A | | 1.7 | 0.30 |
| FDS1 | | | 0.24 | 0.15 | 0.86 | 0.050 | | | 7.2 | 8.4 |
| FDS2 | | | 0.29 | 0.14 | 0.91 | 0.048 | | | 26 | 26 |
| FTS0 | | | 0.64 | 0.18 | 0.65 | 0.089 | | | 2.2 | 5.3 |
| FTL0 | | | 0.82 | 0.21 | 0.90 | 0.045 | | | 1.2 | 6.9 |

644 Table 3: Mean and variance on 500 realizations for the different indicators and test cases. N/A stands for indicators that cannot be computed in
645 the corresponding cases.

646

| | **Porous Cases** | | **Fractured Cases** | |
|---|---|---|---|---|
| | $D_{ic}/L$ | $D_{cc}/L'$ | $D_{ic}/L$ | $D_{cc}/L'$ |
| Full range of variation | 0.12 | 0.66 | 0.73 | 0.40 |
| $\sigma_y^2$ | 0.08 (PG) | 0.1 (PG) | 0.42 ($a$=3.5) | 0.31 (a=3.5) |
| | 0.10 (PF) | 0.55 (PF) | 0.24 ($a$=2.0) | 0.07 ($a$=2.0) |
| $\lambda$ | 0.06 (PG) | 0.09 (PG) | | |
| | 0.04 (PF) | 0.14 (PF) | | |
| $a$ | | | 0.35 ($\sigma_y^2$=0) | 0.30 ($\sigma_y^2$=0) |
| | | | 0.22 ($\sigma_y^2$=3) | 0.05 ($\sigma_y^2$=3) |
| $d$ | | | 0.55 ($a$=3.5) | 0.1 ($a$=3.5) |
| | | | 0.55 ($a$=2.0) | 0.12 ($a$=2.0) |

647 Table 4: Variation range (maximal minus minimal values) of $D_{ic}/L$ and $D_{cc}/L'$ according to
648 porous and fracture parameters. High values in grey are due to transitions from porous-like to
649 fracture-like structures rather than to variations with $\sigma_y^2$.